Received: January 7, 2019

INASS

International Journal of
Intelligent Engineering & Systems

http://www.inass.org/

A Sturdy Nonlinear Hyperspectral Unmixing Algorithm Using Iterative Block-Coordinate Descent Algorithm

Majeti Venkata Sireesha[1]* **Panchala Venkata Naganjaneyulu[2]** **Kaparapu Babulu[3]**

[1]*Department of Electronics and Communication Engineering, Jawaharlal Nehru Technological University, Kakinada, India*
[2]*Sri Mittaplli College of Engineering, Tummalapalem, Guntur, India*
[3]*Jawaharlal Nehru Technological University, Kakinada, India*
* Corresponding author's Email: majetivenkatasireesha@gmail.com

Abstract: To depict the hyperspectral data, here a sturdy mixing model is implemented by employing various perfect spectral signatures mixture, which enhances the generally utilized linear mixture model (LMM) by inserting an extra term that describes the potential nonlinear effects (NEs), which are addressed as additive nonlinearities (NLs) those are disseminated without dense. Accompanying the traditional nonnegativity and sum-to-one restraints underlying to the spectral mixing, this proposed model heads to a novel pattern of sturdy nonnegative matrix factorization (S-NMF) with a term named group sparse outlier. The factorization is presented as an issue of optimization which is later dealt by an iterative block-coordinated descent algorithm (IB-CDA) regarding the updates with maximation-minimisation. Moreover, distinctive hyperspectral mixture models also presented by adopting the considerations like NEs, mismodelling effects (MEs) and endmember variability (EV). The extensive simulation analysis by the implementation of proposed models with their estimation approaches tested on both the synthetic and real-time images. Further, it is also shown that the comparative analysis with the conventional approaches.

Keywords: Spectral unmixing, Hyperspectral images, Linear mixture models, Nonlinear mixture models, Nonlinear spectral unmixing, Endmember variability, Sturdy unmixing, Mismodelling effect and coordinate descent algorithm.

1. Introduction

Hyperspectral image investigation, which renders significant and comprehensive gathered measurements description in several areas of application like spectro-microscopy [1], remote sensing [2], food monitoring [3] and planetology [4] is done by a prefaced concern problem named as spectral unmixing (SU), which was an area of intensive interest over the last two decades. SU is an issue of separating source comprising of reconstructing the material's endmember spectrum which is there in the scene and measuring their symmetries or abundances inside every pixel of HIS. It consists in decomposing P multi-band observations $Y = [y_1, \ldots, y_P]$ into a collection of K individual spectra $R = [r_1, \ldots, r_K]$, called endmembers, and estimating their relative abundances $A = [a_1, \ldots, a_P]$ for each observation [5, 6]. Numerous SU approaches presented in the literatures of geoscience, signal and image processing depends on LMM, $Y \approx RA$. In truth, a good estimation of the physical procedure is rendered by LMM which inherent the observation and has outcome in practicable solvent for numerous applications. Be that as it may, LMM is not suitable for several settings like the models with volumetric dispersing or suggest materials mixture or terrain alleviation. For example, when assuming the scenes like arenaceous, light is mattered to the development of multiple dispersing and assimilation, that led largely NEs. Quite difficult optical modelling is necessitated to deal with the thorough examination of such models and further it is required to recourse

to estimation models to make the issue amenable. For those effects [7, 8], which suffers LMM, an alternate approach is adopted named as nonlinear mixture models (NLMM), which consists of couple of categorizations like first is based on procedure of signal and attempts to build flexile models that can constitutes NLs with a wide range. Second is based on physical and admits the multiple scattered familiar models like polynomial [9] or bilinear [10-14]. Conversely, in an image of remotely sensed those are compiled of vegetation (e.g., trees), photons interaction with several scene elements results in NEs that can be assumed employing bilinear models [15, 16]. As explained in [17], many of these models only differ by the restraints enforced on the bilinear term. Furthermore, to estimate second order NLs with wide range, a polynomial post NLMM is implemented in [18], which has established its capability to depict numerous NEs, in vegetated areas [19]. A general characteristic of such models is that they all integrate an additional term that accounts for NLs to the traditional LMM. However, these models are not without flaws that they necessitate to select a particular pattern of NL, which is highly restricted in practice. A complete overview of NL models with their supported SU algorithms are presented in [20, 21].

In both LMM and NLMM, the endmember matrix (M) are generally assumed fixed in the whole image. This appears as a clear simplification since in many cases, the M spectra vary along the image causing what is known as spectral variability or EV [22, 23]. Spectral variability has been identified as a relevant source of error in abundance estimation and is attracting growing interest in the hyperspectral community [22-24]. In the literature, numerous approaches were implemented to depict this EV and they can be accumulated into couple of major categories where the first one assumes every physical material as known endmember set [25, 26] or reckoned from the data [27, 28]. In addition, numerous M parametric representation is discovered like the every M is multiplied by a picture element subordinate invariant to explicit a variation in illumination in the scene that is noticed [29–31]. The latter category trusts on a numerous M statistical representation which are considered as random vectors with rendered probability dispersions. There are couple of statistical models like normal compositional model (NCM) [32–34] and beta compositional model (BCM) [35] where the first one considers Gaussian dispersions for numerous M and the latter feats the physically naturalistic M range reflectance by attributing them a beta distribution.

Processing of HSI also relate to the MEs, which introduced due to the presence of several physical development like NEs or EV. Be that as it may, these MEs can also be due to the dispersed mistakes in the processing chain of signal. In truth, three stages are employed for operating SU:

- M estimation.
- Employment of endmember extraction approaches (EEA) like vertex component analysis (VCA) [36] and N-FINDR [37] to distinguish M.
- Abundances approximation underneath physical nonnegativity and sum-to-one restraints employing algorithms like entirely restrained least squares [38].

Many studies consider a supervised unmixing scenario which aims at estimating the abundances while if the two first unmixing steps were successfully implemented [38–41]. However, an error on the estimated number of M or in their spectra might results in worse estimation of abundance, which is assumed by several refreshing sturdy SU algorithms those targeted at mitigating the outliers of MEs influence [42].

In a like manner to the NMMs explained above, our proposed model is constructed based on traditional LMM, with the comprehension of an auxiliary linear term that accounts for the impacts of NEs. Hence, the proposed model can be assumed to study any mixture that outcome from the compounding of an additive part MA and the residual term [43]. Indeed, the first stage investigates NEs which can be modelled by assuming a variation to the polynomial term described in literature, that relies only on the spectra of endmember. The second stage assumes the impact of EV by innovating a smooth linear divergence of every known spectra of endmember. Thus, reverse to the NCM explained in some of related articles, the proposed model considers the endmembers in presence of EV with smooth spatial and spectral fluctuation. In addition, the third stage innovated for the residual term which accounted for the MEs with the smooth spectral and spatial properties of corrupting term. Grounded on the residual component analysis (RCA) model [44], global formulation considers the LMM to be profaned by a linear term whose formula can be accommodated to describe for the analyzed development. This residual term is formulated as a compounding of M or abundances contingent the analyzed NEs or EV. The unknown parameter vector joint posterior dispersion is then derived for NEs, EV and MEs by employing the likelihood and

the assumed prior distributions. However, it is quite difficult to calculate the minimum mean square error (MMSE) and maximum a posteriori (MAP) estimators of these parameters from the prevailed joint posteriors, which estimates the MAP by assuming the coordinate descent algorithm (CDA) [45, 46].

The main motivation for introducing proposed approach is to introduce a flexible unmixing method able to analyse a large variety of remotely sensed scenes. It is well admitted that, for most of these images, LMM is a relevant description of the data. For such datasets, resorting to NMMs is not always necessary and may in fact result in inaccurate estimation (due to, e.g., overfitting). Thus, the LMM can be considered as a valid model to describe most of the pixels in a remotely sensed image. Conversely, as illustrated in previous works, the LMM assumption does not support for the areas those are particularly localized, primarily placed at the heterogeneous areas interface. For this restricted number of picture elements, the SU approaches based on LMM failed to recover the materials and their abundances. Of such assumption, our objective is to implement a novel SU model which suits for the both scenarios. However, the work addressed in [47], doesn't operates well with the larger NEs since CDA algorithm updation is quite difficult and it fails to produce good abundance estimate with nonlinear model that was corrupted by additive noise. Therefore, this work aimed at solving these issues and proposed a new CDA algorithm that is named as iterative block coordinate descent algorithm (IB-CDA) that consecutively updates the abundances, the noise variances and the residual terms iteratively. Moreover, S-NMF is employed to minimize the issue where the LMM fails to assume the pixels with nonlinearities. As such, we implemented to decompose the $L \times P$ matrix of the observations with multi-band as $Y \approx RA + N$, where N is a not thick (and non-negative) residual term explicating NEs. The implemented SU models and their reckon algorithms are experimented with both synthetic and real HSI. The incurred outcome is extremely identical and disclose the proposed SU model's possibility with their supported illation algorithms.

The rest of this article is summarized as follows. Section 2 innovates the derivations for the proposed mixture model and its versions to handle with NEs, EV and MEs. Section 3 explains the proposed methodology. Section 4 discusses the simulated results of proposed approaches using synthetic images with known ground truth. and real HSIs. Section V concludes the article and future work also discussed in the same finally reported the references.

2. Mixing model: NL, EV and MEs

The SU expression is grounded on RCA model that is formulated as the summation of LMM and residual term. In practice, the general observation model for the $(L \times 1)$ pixel spectrum $y_{i,j}$ is given by

$$y_{i,j} = \sum_{r=1}^{R} a_{r,i,j} s_{r,i,j} + \varphi_{i,j}(S_{i,j}, a_{i,j}) + e_{i,j} = S_{i,j} a_{i,j} + \varphi_{i,j}(S_{i,j}, a_{i,j}) + e_{i,j} \quad (1)$$

where $a_{i,j}$ is an $(R \times 1)$ abundances vector affiliated with the picture element (i, j), number of endmembers are denoted as R, $e_{i,j} \sim \mathcal{N}(0, \Sigma)$ denotes the linear focused Gaussian noise with a matrix of diagonal covariance $\Sigma = \mathrm{diag}(\sigma^2)$, where $\sigma^2 = [\sigma_1^2, \cdots, \sigma_L^2]^T$ is an $(L \times 1)$ vector comprising the variances of noise with L spectral bands, $S_{i,j}(M) = S_{i,j}$ is the matrix of endmember that relies on every picture element to innovate the impact of EV, the known matrix of endmember that is unchanged denoted as M and residual term is denoted as $\varphi_{i,j}(S_{i,j}, a_{i,j})$, which might rely on the abundances or endmembers to model the impacts of NL or EV. Because of physical restraints, the vector of abundance $a_{i,j} = [a_{r,i,j}, \cdots, a_{R,i,j}]^T$ gratifies the adopting positivity and sum-to-one restraints.

$$a_{r,i,j} \geq 0, \forall r \in \{1, \cdots, R\} \quad \text{and} \quad \sum_{r=1}^{R} a_{r,i,j} = 1 \quad (2)$$

Eq. (1) shows a general model that can be adapted to account for different physical phenomena. The NEs model is designed to deal with the multiple scattering effect that appears in presence of terrain relief, and/or trees. The EV model accounts for the deviation of the endmembers that is commonly observed in presence of vegetation (such as trees or grass), and shadow. It is common to observe the NL and the EV effects simultaneously when analysing a scene. Therefore, a ME model has been proposed to account for both effects. The next sections provide details regarding each of these models.

Nonlinearity Effect: NLMM provide a useful alternative for overcoming the inherent limitations of the LMM. The latter can be inappropriate for some HSI, such as those containing trees, vegetation or urban areas. Bilinear/polynomial models have shown useful results for these scenes by addressing the problem of double scattering effects. In addition to the LMM terms, these models consider second order interactions between M and neglects the effect of the higher order terms. The following

polynomial/bilinear nonlinear model is considered in this article

$$y_{i,j} = c_{i,j} M a_{i,j} + \varphi_{i,j}^{NL}(M) + e_{i,j} \quad (3)$$

where the residual component is similar to [28] as follows:

$$\varphi_{i,j}^{NL}(M) = c_{i,j}^2 \left(\sum_{k=1}^{R-1} \sum_{k'=k+1}^{R} \gamma_{i,j}^{(k,k")} \sqrt{2}\, m_k \odot m_{k'} + \sum_{k=1}^{R} \gamma_{i,j}^{(k)} m_k \odot m_k \right) \quad (4)$$

With $\gamma_{i,j} = \left[\gamma_{i,j}^{(1)}, \cdots, \gamma_{i,j}^{(R)}, \gamma_{i,j}^{(1,2)}, \cdots, \gamma_{i,j}^{(R-1,R)}\right]^T$, $\forall i,j$ is the $(D \times 1)$ vector of positive nonlinearity coefficients, $D = \frac{R(R+1)}{2}$, $\odot$ denotes the Hadamard (term wise) product, k denoted as endmember spectra, $s_{r,i,j} = c_{i,j} m_r, \forall i,j$, with $c_{i,j}$ a pixel dependent illumination coefficient. The model (3) generalizes the model of Somers *et al.* by including an EV illumination parameter $c_{i,j}$ that accounts for the main spectral variation of endmembers. Contrary to the RCA model, model (3) considers physical positive $\gamma_{i,j}$ (the RCA model can be obtained by marginalizing unconstrained $\gamma_{i,j}$). Note also that (3) generalizes the LMM (obtained when $\gamma_{i,j} = 0$, and $c_{i,j} = 1, \forall i,j$) and has a polynomial like form as for the bilinear models. Note finally that model (3) (with no illumination variation) has been studied by Altmann *et al.* when considering a Markov chain Monte-Carlo (MCMC) approach and have shown good performance for processing HSIs. However, the MCMC estimation algorithm was computationally expensive, hence a faster algorithm is considered which utilizes co-ordinate descent algorithm (CDA) described in [47]. Further, CDA is extended to IB-CDA to obtain more effective outcome when LMM fails to assume the pixel NLs.

Endmember Variability Effect: Due to the low spatial resolution of hyperspectral images, the image might represent very large scenes. Therefore, it makes sense to assume that the same material (such as vegetation) might differ with respect to (w. r. t.) the image regions resulting in what it is known as EV. This variability introduces a modification in the shape and the scale of the M spectrum in each pixel, i.e., $s_{i,j}$ depends on the pixel location.

Despite the fact that these spectra are affiliated with the similar material, they show some differences which is known as EV effect. To highlight this effect, we compute the average spectrum in each spectral band, and assume that EV is obtained by computing the difference between the spectra and the average spectrum. Therefore, to account for the shape variability of each endmember, each endmember can be approximated by the sum of a fixed spectrum and a smooth spectral function representing EV. This smooth function can be modelled by a parametric approach such as spline, or a statistical approach as Gaussian process. Here, following EV model considered

$$s_{r,i,j} = m_r + k_{r,i,j} \quad (5)$$

where $k_{r,i,j}$ is a smooth spectral function, which leads to

$$y_{i,j} = M a_{i,j} + \varphi_{i,j}^{EV}(a_{i,j}) + e_{i,j} \quad (6)$$

Where

$$\varphi_{i,j}^{EV}(a_{i,j}) = \sum_{r=1}^{R} a_{r,i,j} k_{r,i,j} \quad (7)$$

Note that Eq. (7) does not consider an illumination parameter $c_{i,j}$ since its effect can be included in the smooth function $k_{r,i,j}$. Model Eq. (7) relates to state-of-the-art models as follows: (i) it generalizes the LMM that can be retrieved for $k_{r,i,j} = 0_L, \forall i,j$, (ii) it generalizes the model [30] by including the effect of shape variability, and (iii) it has a similar formulation as in [48] while accounting for the spectral smoothness of the residuals. Note finally that in the special case where $k_{r,i,j}$ is Gaussian distributed (Gaussian process), the model Eq. (6) will improve the GNCM by including the smooth behaviour of EV (model Eq. (6) is closely related to the GNCM that can be obtained by marginalizing $s_{i,j}$ when considering a Bayesian approach).

Mismodelling Effects (ME) or Outliers: The LMM is widely used because of its simplicity. As previously shown, there is a lot of situations where the LMM is not valid because of the presence of variability, NL or MEs due to the signal processing chain errors. This section accounts for MEs or the presence of outliers by considering a residual term that shows spatial and spectral correlations. The observation model is given by

$$y_{i,j} = c_{i,j} M a_{i,j} + \varphi_{i,j}^{ME}(M) + e_{i,j} \quad \text{with} \quad \varphi_{i,j}^{ME} = d_{i,j} \quad (8)$$

Where a function of smooth spectral is denoted as $d_{i,j}$. Similarly, to the previous models, Eq. (8)

reduces to the LMM when $d_{i,j} = 0_L$, and $c_{i,j} = 1, \forall i,j$. Note that other models have been introduced in the literature to account for the effect of outliers that proposed spatial/spectral correlated outliers by considering discrete Markov random fields (MRF). Note that Eq. (8) be a special case of the EV model Eq. (7) when $k_{r,i,j} = k_{r\prime,i,j}, \forall r, r'$ and $c_{i,j} = 1$, i.e., the same variability is affecting the different M. Note also that the NL model Eq. (4) reduces to Eq. (8) if $\gamma^{(k,k\prime)} = \gamma, \forall k, k'$ since the spectra $m_k \odot m_{k\prime}, \forall, k, k'$ are generally smooth. However, Eq. (8) is more flexible since it does not consider the positivity constraint (mainly to account for EV).

Algorithm 1: CDA

1: Estimate M using an EEA (such as VCA [], N-FINDR [], …)
2: Initialize parameters $A^{(0)}$ (SUNSAL-FCLS), $\Gamma^{(0)}$, $K^{(0)}$, $D^{(0)}$, $c^{(0)}$, $\sum^{(0)}$, $\varepsilon^{(0)}$ and t
3: conv = 0
4: **while** conv = 0 **do**
5: Update $A^{(t)}$ with SUNSAL-FCLS
6: CDA-NL: Update $\Gamma^{(t)}$ with SUNSAL-FCLS
7: CDA-EV: Update $K^{(t)}$ by standard least squares
8: CDA-ME: Update $D^{(t)}$ by standard least squares
9: CDA-NL and CDA-ME: Update $(\varepsilon, \omega)^{(t)}$ by standard least squares
10: Update $\sum^{(t)}$
11: CDA-ME: Update $c^{(t)}$ by standard least squares
12: CDA-NL: Update $c^{(t)}$ by the resolution of 3rd order polynomial
13: Set conv = 1, if the convergence criterion is satisfied
14: $t = t + 1$
15: **end while**

3. Proposed methodology

3.1 Model design

$$y_{i,j} \approx \sum_{r=1}^{R} a_{r,i,j} m_r + n_{i,j} \quad (9)$$

The matrix formulation for above equation is given by

$$Y \approx RA + N \quad (10)$$

This Eq. (9) generalizes most of the bilinear mixing models that have been widely used to analyse hyperspectral scenes acquired over multi-layered areas by remote sensors. This specific context has been extensively studied in the literature, for planetary and Earth science to characterize vegetation or urban canopies.

The approximation symbol in Eq. (9) and Eq. (10) underlies the minimization of a measure of dissimilarity $D(Y|RA + N)$. The measure of dissimilarity is such that $D(A|B) = \sum_{ij} d(a_{ij}|b_{ij})$, where $d(x|y)$ is either the squared Euclidean distance (SED) or the Kullback-Leibler divergence (KLD). We address these two measures of dissimilarity because they are the most commonly used in non-negative matrix factorization (NMF). The SED is the more common one in hyperspectral unmixing, but recent papers have also pointed the benefits of using the KLD. As will be discussed in conclusion section, the methodology presented in the paper could also accommodate other measures of fit such as the more general β-divergence. The matrices Y, R and A are nonnegative by nature and we assume the abundance coefficients to sum to one, i.e.,

$$a_{i,j} \in \mathbb{S}^R \stackrel{\text{def}}{=} \{a \in \mathbb{N}^R | a_r \geq 0, \sum_{r=1}^{R} a_r = 1\} \quad (11)$$

as commonly assumed in most hyperspectral data models. In this work, we assume the nonlinear component $n_{i,j}$ to be nonnegative as well, like in the bilinear models and the polynomial model with constructive interferences. This assumption allows a fair comparison with the latter works, which inspired us the proposed methodology, and is physically well-motivated for multi-layered models (scenes with multiple reflections).

As discussed in the introduction, we expect $n_{i,j}$ to be often zero, i.e., pixels to follow the standard LMM in general. For pixels where the LMM assumption fails, nonlinearities will become "active" and $n_{i,j}$ will become nonzero. This amounts to say that the energy vector in sparse.

$$e = \left[\left\|n_{r,1}\right\|_2, \cdots, \left\|n_{r,i,j}\right\|_2\right] \quad (12)$$

In Eq. (12), $\|\cdot\|_2$ denotes the Euclidean norm. Sparsity can be routinely enforced by ℓ_1 - regularization, as done next.

In light of earlier section, our objective is to solve the minimization problem defined by

$$\min_{M,A,N} J(R,A,N) = D(Y|RA + N) + \lambda \|N\|_{2,1}$$
$$s.t. R \geq 0, A \geq 0, N \geq 0 \text{ and } \left\|a_{i,j}\right\|_1 = 1 \quad (13)$$

Where λ is the nonnegative penalty weight, $A \geq 0$ denotes coefficients nonnegativity of A and $\|\cdot\|_{2,1}$ is the so called $\ell_{2,1}$-norm defined by

$$\|N\|_{2,1} = \|e\|_1 = \sum_{i,j=1}^{P} \left\|n_{i,j}\right\|_2 \quad (14)$$

Eq. (13) defines a sturdy NMF (S-NMF) problem. S-NMF is a nonnegative variant of robust PCA [48] which has appeared in different forms in the literature. In [50], the outlier term N is nonnegative and penalized by the ℓ_1-norm. In [51] and [52], N is real-valued and penalized by ℓ_1 and $\ell_{1,2}$-norms, respectively. In [53], the $\ell_{2,1}$-norm of $(Y - RA)$ is minimized (noise-free scenario). A so-called S-NMF approach was introduced for the reconstruction of reflectance spectra in [54]; however, the term "sturdy" there refers to a different feature, namely the use of a data-fitting term (the hypersurface cost function) that is less sensitive to outlier observations than the traditional SED, for the computation of a regular NMF $Y \approx RA$. Note finally that other articles have addressed hyperspectral unmixing with regular NMF (i.e., in the standard linear model). To the best of our knowledge, the formulation of S-NMF described by Eq. (5), where N is nonnegative and penalized by the $\ell_{2,1}$ norm (and where the abundances sum to one), is entirely novel. Furthermore, previous works [49-52] have only considered S-NMF with the SED, i.e., $D(Y|RA + N) = \|Y - MA - N\|_2^2$, while we here also address the case of the KLD.

In order to solve the S-NMF minimization problem defined at Eq. (5), we present an iterative block-coordinate descent algorithm that updates each of the parameters M, A and N in turn. Each parameter is updated conditionally upon the current value of the other parameters and such that the objective function is decreased. This is the updating scheme employed by virtually all NMF algorithms. Unfortunately, given the non-convexity of the objective function $J(R, A, N)$, this strategy can return local solutions and proper initialization is required. The updates of the parameters are described next. In short, the parameters R and N are updated via majorization-minimization (MM). Generally speaking, MM consists in optimizing an easier-to minimize tight upper-bound of the original objective function. The parameter A is updated using a heuristic scheme that has proven to work well in the literature. All the updates turn out to be "multiplicative", i.e., such that the new update is obtained by term-to-term multiplying the previous update by a nonnegative matrix, hence automatically preserving the nonnegativity of the estimates through iterations. The resulting algorithm has linear complexity $O(LKP)$ (in flops) per iteration.

Algorithm 2: S-NMF with IB-CDA

1: Initialize R, A and N
2: Set $\beta = 1$ *or* 2, λ and convergence tolerance 'tol'
3: $S = RA$
4: $\hat{Y} = S + N$
5: **while** $err \geq tol$, **do**
% Update the term N
6: $R \leftarrow R\left[\frac{Y.\hat{Y}^{.(\beta-2)}}{\hat{Y}^{.(\beta-1)} + \lambda\, N\, diag\left[\left\|n_{r,1}\right\|_1, \cdots, \left\|n_{r,i,j}\right\|_1\right]^{-1}}\right]$
7: $\hat{Y} \leftarrow S + N$
% Update abundance A
8: $A \leftarrow A.\frac{M^T\left(Y.\hat{Y}^{.(\beta-2)} + 1_{K,L}\left(S.\hat{Y}^{.(\beta-1)}\right)\right)}{M^T\left(\hat{Y}^{.(\beta-1)} + 1_{K,L}\left(S.Y.\hat{Y}^{.(\beta-2)}\right)\right)}$
9: $A \leftarrow A\ \text{diag}\left[\left\|a_{r,1}\right\|_1, \cdots, \left\|a_{r,i,j}\right\|_1\right]^{-1}$
10: $S \leftarrow RA$
11: $Y \leftarrow S + N$
% Update endmember M
12: R$\leftarrow R.\left[\frac{\left(Y.\hat{Y}^{.(\beta-2)}\right)A^T}{\left(\hat{Y}^{.(\beta-1)}\right)A^T}\right]$
13: $S \leftarrow RA$
14: $Y \leftarrow S + N$
15: Compute the objective function relative decrease 'err' (or any other convergence criterion).
16: **end while**

In Algorithm 2, all operators preceded by a dot '.' are entry wise MATLAB-like operations and fraction bars shall be taken term-to-term as well. Additionally, $1_{M,N}$ denotes the $M \times N$ matrix with coefficients equal to 1.

3.2 Setting the value of λ

The hyperparameter λ controls the trade-off between the data-fitting term $D(Y|RA + N)$ and the penalty term $\|N\|_{2,1}$. Setting the "right" value of λ is a difficult task, like in any other so-called variational approach that involves a regularization term. We describe in this paragraph a rule of thumb for choosing λ in a plausible range of values. Our approach is based on the method of moments. It consists in interpreting the objective function (5) as a joint likelihood and in matching the empirical mean of the data with its prior expectation in the statistical model. The SED and the KLD are "pseudo-likelihood" for probabilistic models (Gaussian and Poisson, respectively) such that $E[Y|RA + N] = RA + N$. In the same analogy, the term $\lambda\|N\|_{2,1}$ can be interpreted as a log-prior term.

Using some results from [55], the corresponding prior distribution $p(n_{r,i,j}|\lambda)$ for each column of R can be obtained as a scale mixture of conditionally independent half-Normal distributions, with a Gamma distribution assigned to the scale parameter.

4. Results and discussion

4.1 Results on synthetic data

This section evaluates the performance of the proposed algorithms with synthetic data. The first part introduces the criteria used for the evaluation of the unmixing quality. In the second part, we evaluate and compare the performance of the proposed algorithms with the state-of-the-art algorithms when considering different unmixing scenarios.

4.1.1. Evaluation criteria

For synthetic images, the abundances are known and the unmixing quality can be evaluated by using the root mean square error (RMSE):

$$RMSE(A) = \sqrt{\frac{1}{XR}\sum_{x=1}^{X}\|a_x - \hat{a}_x\|^2} \qquad (15)$$

The unmixing performance can also be evaluated by considering the reconstruction error (RE) and spectral angular mapper (SAM):

$$RE = \sqrt{\frac{1}{X\,L}\sum_{x=1}^{X}\left\|\hat{Y}_x - Y_x\right\|^2} \qquad (16)$$

$$SAM = \frac{1}{X}\sum_{x=1}^{X} arccos\left(\frac{\hat{Y}_x^T Y_x}{\|Y_x\|\|\hat{Y}_x\|}\right) \qquad (17)$$

Where $arccos(\cdot)$ is the function of inverse cosine and Y_x, $\hat{Y}_x$ are the measured and estimated x^{th} pixel spectra.

4.1.2. Proposed algorithms evaluation

This section evaluates the performance of the proposed unmixing algorithms when considering different mixture models. Four synthetic images of size 100 × 100 pixels and L = 207 spectral bands have been generated using R = 3 endmembers corresponding to spectral signatures available in the ENVI software library [56]. All images have been corrupted by $i.i.d.$ Gaussian noise (with SNR=25 dB) for a fair comparison with SU algorithms using this assumption. Distinctive unmixing schemes are employed for processing of these images that are equate to the proposed models. For every model, it is considered that there are known endmembers and had assumed spectra of ENVI is employed to innovate the images.

Table 1. Results on synthetic data

Method	RMSE ($\times 10^{-2}$)	RE ($\times 10^{-2}$)	SAM($\times 10^{-2}$)
FCLS [38]	24.76	15.74	10.64
SUNSAL-CLS [39]	16.55	4.17	7.57
AEB [28]	45.72	3.05	6.46
CDA-EV [47]	16.59	3.34	6.64
CDA-ME [47]	6.61	2.89	6.17
CDA-NL [47]	3.86	2.86	6.16
Proposed method	**1.57**	**1.20**	**4.9**

Table 1 shows the obtained results when considering synthetic data image. The superior performance is obtained by proposed SU model and it is sturdier against various NLs since it achieved the best value of RMSE compared to the conventional SU models. Further, it also achieved the best outcome for the values of RE and SAM also which indicates that the proposed SU model is suitable for the different physical developments like NEs, EV or MEs.

4.2 Results on real data

In this section we apply S-NMF with IB-CDA to real hyperspectral datasets and discuss the results.

4.2.1. Description of dataset

We consider two real hyperspectral images that have been chosen because of availability of partial ground truth. The first image was acquired over Moffett Field, CA, in 1997, by the Airborne Visible Infrared Imaging Spectrometer (AVIRIS) [57]. Water absorption bands have been removed from the 224 spectral bands, leading to L = 189 spectral bands ranging from 0.4μm to 2.5μm with a nominal bandwidth of 10nm. The scene of interest, of size of 50×50 pixels, consists of a part of lake and a coastal area composed of soil and vegetation. This dataset will be referred to as the "Moffett" image in the following and is depicted in Fig. 3(a).

The second considered dataset was acquired by the Hyspex hyperspectral scanner over Villelongue, France, in 2010. The sensed spectral domain consists of L = 160 spectral bands ranging from 0.4μm to 1.0μm. This image consists of a forested area where 12 vegetation species have been identified, during the Madonna project. The sub-

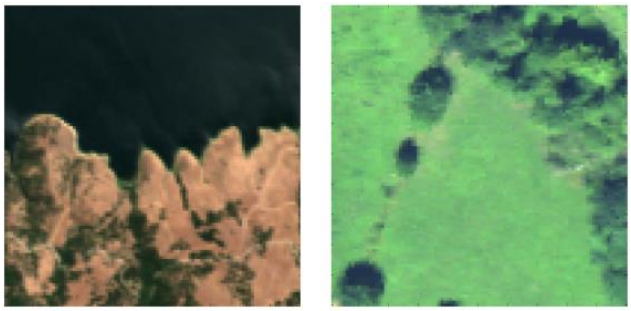

(a) (b)

Figure. 3 Real HIS: (a) Moffett image and (b) Madonna image

image of interest, of size of 50×50 pixels, is known to be mainly composed of oak and chestnut trees, with an additional unknown non-plantedtree endmember. This dataset will be referred to as the "Madonna" image in the following and is depicted in Fig. 3 (b).

4.2.2. Unmixing performance

The abundances of each image have been estimated by the considered unmixing algorithms. There are four abundance maps (denoted as Abund1, Abund2, Abund3 and Abund4 in Fig. 4) since we assumed four endmembers i.e., soil, water, tree and shadow. Fig. 4 shows the obtained results of four abundance maps of various unmixing algorithms such as FCLS [38], SUNSAL [39], UsGNCM [24], CDA-NL [47], CDA-ME [47] and proposed unmixing algorithm for the Madonna image. Note that a white (black) pixel indicates a large (small) proportion of the corresponding materials. Except FCLS, the considered algorithms show similar abundance maps. The behavior of FCLS is due to the presence of a high illumination variation for this image. In addition, some nonlinearity can be interpreted as an illumination variability (as already shown when analysing synthetic data) leading to high values for the parameter c. The unmixing performance which can also be compared by considering the RMSE, RE, SAM and even spectral inverse divergence (SID) as shown in Table 2. Considering the Madonna image, the best values of obtained metrics are highlighted in bold letter for better perception. The best performance on the Madonna image are obtained by the proposed S-NMF with IB-CDA while we obtain good results when considering the algorithms including EV such as CDA-ME [47].

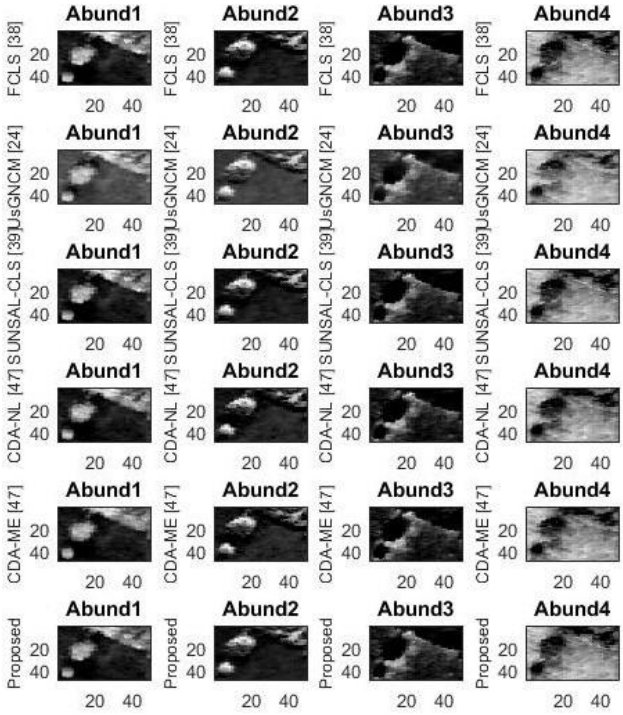

Figure. 4 Estimated abundance maps with different algorithms for the Madonna image, grass, shadow, soil, and water

Table. 2 Results on Madonna image

Method	**RMSE** ($\times 10^{-2}$)	**RE** ($\times 10^{-3}$)	**SAM**($\times 10^{-2}$)	**SID**
FCLS [38]	--	6.3	2.7	2.88
SUNSAL-CLS [39]	--	6.2	2.6	--
UsGNCM [24]	12.03	8.9	2.7	0.42
CDA-NL [47]	4.81	5.84	2.7	**0.04**
CDA-EV [47]	--	6.0	**2.5**	--
CDA-ME [47]	5.52	3.81	2.6	0.06
Proposed method	**2.19**	**3.81**	2.8	0.07

These results suggest the presence of a higher variability effect than nonlinearity in the Madonna image. Note finally that the proposed algorithm shows a superior performance with comparison to the UsGNCM [24], CDA-NL [47] and CDA-ME [47] when there are distinctive nonlinearities influencing data. Furthermore, the best abundance estimation also obtained by the proposed S-NMF with IB-CDA since the best outcomes of RMSE and RE are achieved by the proposed algorithm.

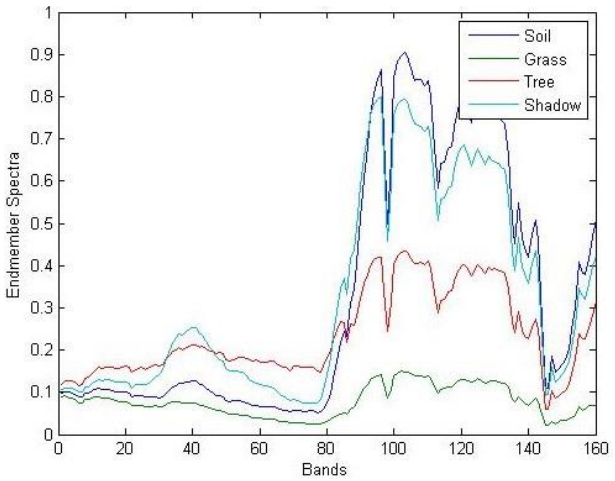

Figure. 5 The estimated $R = 4$ endmembers of Madonna image

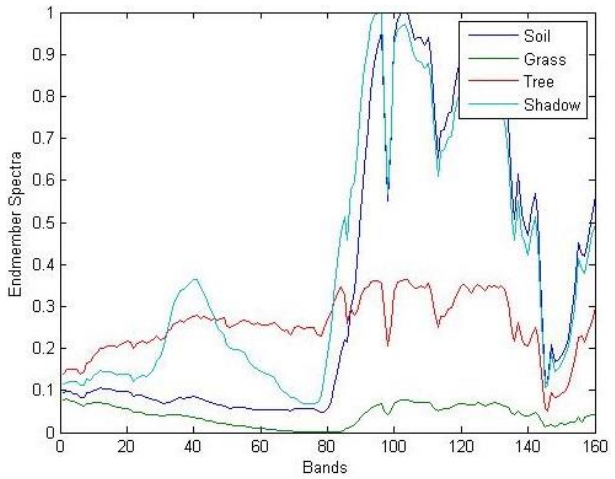

Figure. 6 The estimated $R = 4$ endmembers of Madonna image with UsGNCM [24]

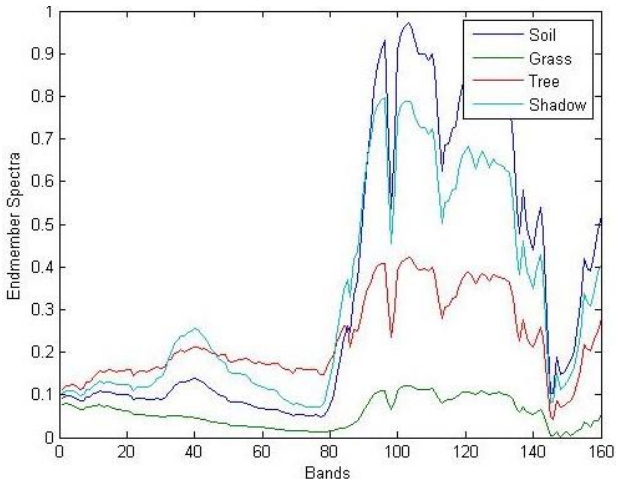

Figure. 7 The estimated $R = 4$ endmembers of Madonna image with proposed S-NMF with IB-CDA

Fig. 5 depicts that the endmember variability of original model whereas the UsGNCM model [24] is disclosed in Fig. 6 while the proposed unmixing model is depicted in Fig. 7, which concludes that the estimated endmember variability of proposed model is almost similar to that of original one where as the obtained endmember variability of UsGNCM [24] is over headed the original model which in results the NLs and MEs in the pixels of hyperspectral image. Performance comparison of obtained evaluation criteria values is demonstrated in Fig. 8, which are demonstrated in Table 2. It is shown that the best values of RMSE and RE are obtained by proposed unmixing model which disclose that the sturdiness and accurate abundance of HIS with NEs, EV or MEs, where the conventional unmixing models failed to get the approximate abundance with sturdy against the NEs, EV or MEs.

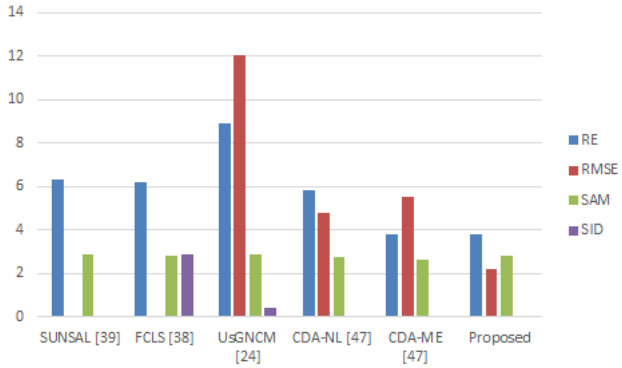

Figure. 8 Performance comparison of unmixing models with evaluation criteria

5. Conclusions

In this paper we have presented a new mixing model to describe hyperspectral data. In contrast with state-of-the-art literature on nonlinear hyperspectral unmixing, our approach does not require the specification of a model of nonlinearity. The resulting unmixing problem was formulated as a new form of sturdy NMF problem, for which we developed a simple and effective iterative block-coordinate descent algorithm that involves multiplicative updates. Further, we addressed three hyperspectral mixture models for supervised hyperspectral unmixing. The three models were introduced under a general formulation that can be adapted to account for nonlinearity effects, endmember variability or mismodelling effects. The proposed algorithms showed good performance when processing synthetic data generated with the linear model or other more sophisticated models. Results on real data confirmed the good performance of the proposed algorithms and showed their ability to extract different features in the observed scenes. In addition, parameters like RE, RMSE, SAM and SID also calculated to disclose the effectiveness of proposed unmixing algorithm over

the existing approaches. Based on these values only the proposed three unmixing models are concluded that they are sturdy against the NLs, EV and MEs.

Future work includes that the denoising of hyperspectral images for an effective unmixing of hyperspectral images with more efficacious mixing models.

References

[1] N. Dobigeon and N. Brun, "Spectral mixture analysis of EELS spectrum images", *Ultramicroscopy*, Vol. 120, pp. 25–34, 2012.

[2] G. P. Asner and K. B. Heidebrecht, "Spectral unmixing of vegetation, soil and dry carbon cover in arid regions: comparing multispectral and hyperspectral observations", *Int. J. Remote Sens.*, Vol. 23, No. 19, pp. 3939–3958, 2002.

[3] A. A. Gowen, C. P. O'Donnell, P. Cullen, G. Downey, and J. M. Frias, "Hyperspectral imaging: an emerging process analytical tool for food quality and safety control", *Trends in Food Science & Technology*, Vol. 18, No. 12, pp. 590–598, 2007.

[4] K. E. Themelis, F. Schmidt, O. Sykioti, A. A. Rontogiannis, K. D. Koutroumbas, and I. A. Daglis, "On the unmixing of MEx/OMEGA hyperspectral data", *Planetary and Space Science*, Vol. 68, No. 1, pp. 34–41, 2012.

[5] N. Keshava and J. F. Mustard, "Spectral unmixing", *IEEE Signal Process. Mag.*, Vol. 19, No. 1, pp. 44–57, 2002.

[6] J. M. Bioucas-Dias, A. Plaza, N. Dobigeon, M. Parente, Q. Du, P. Gader, and J. Chanussot, "Hyperspectral unmixing overview: Geometrical, statistical, and sparse regression-based approaches", *IEEE J. Sel. Topics Appl. Earth Observations and Remote Sens.*, Vol. 5, No. 2, pp. 354–379, 2012.

[7] R. Heylen, M. Parente, and P. Gader, "A review of nonlinear hyperspectral unmixing methods", *IEEE J. Sel. Topics Appl. Earth Observat. Remote Sens.*, Vol. 7, No. 6, pp. 1844–1868, 2014.

[8] N. Dobigeon, J.-Y. Tourneret, C. Richard, J. C. M. Bermudez, S. McLaughlin, and A. O. Hero, "Nonlinear unmixing of hyperspectral images: Models and algorithms", *IEEE Signal Process. Mag.*, Vol. 31, No. 1, pp. 82–94, 2014.

[9] Y. Altmann, A. Halimi, N. Dobigeon, and J.-Y. Tourneret, "Supervised nonlinear spectral unmixing using a postnonlinear mixing model for hyperspectral imagery", *IEEE Trans. Image Process.*, Vol. 21, No. 6, pp. 3017–3025, 2012.

[10] A. Halimi, Y. Altmann, N. Dobigeon, and J.-Y. Tourneret, "Nonlinear unmixing of hyperspectral images using a generalized bilinear model", *IEEE Trans. Geosci. Remote Sens.*, Vol. 49, No. 11, pp. 4153–4162, 2011.

[11] A. Halimi, Y. Altmann, N. Dobigeon, and J.-Y. Tourneret, "Unmixing hyperspectral images using the generalized bilinear model", In: *Proc. of IEEE Int. Geosci. Remote Sens. Symp.*, pp. 1886–1889, 2011.

[12] J. M. P. Nascimento and J. M. Bioucas-Dias, "Nonlinear mixture model for hyperspectral unmixing", In: *Proc. of SPIE*, Vol. 7477, p. 74770I, 2009.

[13] W. Fan, B. Hu, J. Miller, and M. Li, "Comparative study between a new nonlinear model and common linear model for analysing laboratory simulated-forest hyperspectral data", *Int. J. Remote Sens.*, Vol. 30, No. 11, pp. 2951–2962, 2009.

[14] I. Meganem, P. Deliot, X. Briottet, Y. Deville, and S. Hosseini, "Linear-quadratic mixing model for reflectances in urban environments", *IEEE Trans. Geosci. Remote Sensing*, Vol. 52, No. 1, pp. 544–558, 2014.

[15] B. Somers, K. Cools, S. Delalieux, J. Stuckens, D. V. der Zande, W. W. Verstraeten, and P. Coppin, "Nonlinear hyperspectral mixture analysis for tree cover estimates in orchards", *Remote Sens. Environment*, Vol. 113, pp. 1183–1193, 2009.

[16] B. Somers, L. Tits, and P. Coppin, "Quantifying nonlinear spectral mixing in vegetated areas: computer simulation model validation and first results", *IEEE J. Sel. Topics Appl. Earth Observations and Remote Sens.*, Vol. 7, No. 6, pp. 1956–1965, 2014.

[17] Y. Altmann, N. Dobigeon, and J.-Y. Tourneret, "Bilinear models for nonlinear unmixing of hyperspectral images", In: *Proc. of IEEE GRSS Workshop Hyperspectral Image SIgnal Process.: Evolution in Remote Sens.*, pp. 1–4, 2011.

[18] Y. Altmann, A. Halimi, N. Dobigeon, and J.-Y. Tourneret, "Supervised nonlinear spectral unmixing using a post-nonlinear mixing model for hyperspectral imagery", *IEEE Trans. Image Process.*, Vol. 21, No. 6, pp. 3017–3025, 2012.

[19] N. Dobigeon, L. Tits, B. Somers, Y. Altmann, and P. Coppin, "A comparison of nonlinear mixing models for vegetated areas using simulated and real hyperspectral data", *IEEE J. Sel. Topics Appl. Earth Observations and Remote Sens.*, Vol. 7, No. 6, pp. 1869–1878, 2014.

[20] N. Dobigeon, J.-Y. Tourneret, C. Richard, J. C. M. Bermudez, S. McLaughlin, and A. O. Hero, "Nonlinear unmixing of hyperspectral images: Models and algorithms", *IEEE Signal Process. Mag.*, Vol. 31, No. 1, pp. 89–94, 2014.

[21] R. Heylen, M. Parente, and P. Gader, "A review of nonlinear hyperspectral unmixing methods", *IEEE J. Sel. Topics Appl. Earth Observations and Remote Sens.*, Vol. 7, No. 6, pp. 1844–1868, 2014.

[22] Somers, G. P. Asner, L. Tits, and P. Coppin, "Endmember variability in spectral mixture analysis: A review", *Remote Sens. Environ.*, Vol. 115, No. 7, pp. 1603–1616, 2011.

[23] A. Zare and K. Ho, "Endmember variability in hyperspectral analysis: Addressing spectral variability during spectral unmixing", *IEEE Signal Process. Mag.*, Vol. 31, No. 1, pp. 95–104, 2014.

[24] A. Halimi, N. Dobigeon, and J.-Y. Tourneret, "Unsupervised unmixing of hyperspectral images accounting for endmember variability", *IEEE Trans. Image Process.*, Vol. 24, No. 12, pp. 4904–4917, Dec. 2015.

[25] A. Roberts, M. Gardner, R. Church, S. Ustin, G. Scheer, and R. O. Green, "Mapping chaparral in the Santa Monica Mountains using multiple endmember spectral mixture models", *Remote Sens. Environ.*, Vol. 65, No. 3, pp. 267–279, 1998.

[26] A. Bateson, G. P. Asner, and C. A. Wessman, "Endmember bundles: A new approach to incorporating endmember variability into spectral mixture analysis", *IEEE Trans. Geosci. Remote Sens.*, Vol. 38, No. 2, pp. 1083–1094, 2000.

[27] M. Goenaga, M. Torres-Madronero, M. Velez-Reyes, S. J. Van Bloem, and J. D. Chinea, "Unmixing analysis of a time series of hyperion images over the Guánica dry forest in Puerto Rico", *IEEE J. Sel. Topics Appl. Earth Observat. Remote Sens.*, Vol. 6, No. 2, pp. 329–338, 2013.

[28] B. Somers, M. Zortea, A. Plaza, and G. Asner, "Automated extraction of image-based endmember bundles for improved spectral unmixing", *IEEE J. Sel. Topics Appl. Earth Observat. Remote Sens.*, Vol. 5, No. 2, pp. 396–408, 2012.

[29] M. P. Nascimento and J. M. Bioucas Dias, "Does independent component analysis play a role in unmixing hyperspectral data", *IEEE Trans. Geosci. Remote Sens.*, Vol. 43, No. 1, pp. 175–187, 2005.

[30] M. A. Veganzones, L. Drumetz, G. Tochon, M. D. Mura, A. Plaza, J. Bioucas-Dias, and J. Chanussot, "A new extended linear mixing model to address spectral variability", In: *Proc. of IEEE Workshop Hyperspectral Image Signal Process., Evol. Remote Sens.*, 2014.

[31] G. A. Shaw and H.-H. K. Burke, "Spectral imaging for remote sensing", *Lincoln Lab. J.*, Vol. 14, No. 1, pp. 3–28, 2003.

[32] O. Eches, N. Dobigeon, C. Mailhes, and J.-Y. Tourneret, "Bayesian estimation of linear mixtures using the normal compositional model. Application to hyperspectral imagery", *IEEE Trans. Image Process.*, Vol. 19, No. 6, pp. 1403–1413, 2010.

[33] Zare, P. Gader, and G. Casella, "Sampling piecewise convex unmixing and endmember extraction", *IEEE Trans. Geosci. Remote Sens.*, Vol. 51, No. 3, pp. 1655–1665, 2013.

[34] D. Stein, "Application of the normal compositional model to the analysis of hyperspectral imagery", In: *Proc. of IEEE Workshop Adv. Techn. Anal. Remotely Sensed Data*, pp. 44–51, 2003.

[35] X. Du, A. Zare, P. Gader, and D. Dranishnikov, "Spatial and spectral unmixing using the beta compositional model", *IEEE J. Sel. Topics Appl. Earth Observat. Remote Sens.*, Vol. 7, No. 6, pp. 1994–2003, 2014.

[36] M. P. Nascimento and J. M. Bioucas-Dias, "Vertex component analysis: A fast algorithm to unmix hyperspectral data", *IEEE Trans. Geosci. Remote Sens.*, Vol. 43, No. 4, pp. 898–910, 2005.

[37] Winter, "Fast autonomous spectral end-member determination in hyperspectral data", In: *Proc. of the 13th Int. Conf. Appl. Geologic Remote Sens.*, Vol. 2, pp. 337–344, 1999.

[38] C. Heinz and C.-I. Chang, "Fully constrained least-squares linear spectral mixture analysis method for material quantification in hyperspectral imagery", *IEEE Trans. Geosci. Remote Sensing*, Vol. 29, No. 3, pp. 529–545, 2001.

[39] J. Bioucas-Dias and M. A. T. Figueiredo, "Alternating direction algorithms for constrained sparse regression: Application to hyperspectral unmixing", In: *Proc. of the 2nd Workshop Hyperspectral Image Signal Process., Evol. Remote Sens.*, pp. 1–4, 2010.

[40] Y. Altmann, M. Pereyra, and S. McLaughlin, "Bayesian nonlinear hyperspectral unmixing with spatial residual component analysis", *IEEE Trans. Image Process.*, Vol. 1, No. 3, pp. 174–185, 2015.

[41] J. Chen, C. Richard, and P. Honeine, "Nonlinear unmixing of hyperspectral data based on a linear-mixture/nonlinear-fluctuation model", *IEEE Trans. Signal Process.*, Vol. 61, No. 2, pp. 480–492, 2013.

[42] Y. Altmann, S. McLaughlin, and A. Hero, "Robust linear spectral unmixing using anomaly detection", *IEEE Trans. Comput. Imag.*, Vol. 1, No. 2, pp. 74–85, 2015.

[43] R. Close, P. Gader, J. Wilson, and A. Zare, "Using physics-based macroscopic and microscopic mixture models for hyperspectral pixel unmixing", In: *Proc. of SPIE Algorithms and Technologies for Multispectral, Hyperspectral, and Ultraspectral Imagery XVIII*, S. S. Shen and P. E. Lewis, Eds., vol. 8390. Baltimore, Maryland, USA: SPIE, 2012.

[44] A. A. Kalaitzis and N. D. Lawrence, "Residual component analysis", In: *Proc. of ICML*, pp. 1–3, 2012.

[45] J. Sigurdsson, M. O. Ulfarsson, and J. R. Sveinsson, "Hyperspectral unmixing with l_q -regularization", *IEEE Trans. Geosci. Remote Sens.*, Vol. 52, No. 11, pp. 6793–6806, 2014.

[46] A. Halimi, C. Mailhes, J.-Y. Tourneret, and H. Snoussi, "Bayesian estimation of smooth altimetric parameters: Application to conventional and delay/Doppler altimetry", *IEEE Trans. Geosci. Remote Sens.*, Vol. 54, No. 4, pp. 2207–2219, 2016.

[47] A. Halimi and P. Honeine, "Hyperspectral unmixing in presence of endmember variability, nonlinearity and mismodelling effects", *IEEE Trans. Imag. Proc.*, Vol. 25, No. 10, pp. 4565-4579, 2016.

[48] P.-A. Thouvenin, N. Dobigeon, and J.-Y. Tourneret, "Hyperspectral unmixing with spectral variability using a perturbed linear mixing model", *IEEE Trans. Signal Process.*, Vol. 64, No. 2, pp. 525–538, 2016.

[49] J. Cand`es, X. Li, Y. Ma, and J. Wright, "Robust principal component analysis", *Journal of ACM*, Vol. 58, No. 1, pp. 1–37, 2009.

[50] P. Sprechmann, A. Bronstein, and G. Sapiro, "Real-time online singing voice separation from monaural recordings using robust low-rank modelling", In: *Proc. of Int. Soc. Music Information Retrieval Conf.*, 2012.

[51] L. Zhang, Z. Chen, M. Zheng, and X. He, "Robust nonnegative matrix factorization", *Front. Electr. Electron. Eng. China*, Vol. 6, No. 2, pp. 192–200, 2011.

[52] B. Shen, L. Si, R. Ji, and B. Liu, "Robust nonnegative matrix factorization via L_1 norm regularization", *ArXiv preprint*, 2012.

[53] D. Kong, C. Ding, and H. Huang, "Robust nonnegative matrix factorization using $L_{2,1}$-norm", *In: Proc. of the 20th ACM Int. Conf. Information and Knowledge Management*, pp. 673–682, 2011.

[54] A. Ben Hamza and D. J. Brady, "Reconstruction of reflectance spectra using robust nonnegative matrix factorizations," *IEEE Trans. Signal Process.*, Vol. 54, pp. 3637–3642, 2006.

[55] A. Lee, F. Caron, A. Doucet, and C. Holmes, "A Hierarchical Bayesian Framework for Constructing Sparsity-inducing Priors", *arXiv.org*, 2010.

[56] ENVI User's Guide Version 4.0, Boulder, CO, USA, RSI Research Systems Inc., Sep. 2003.

[57] Jet Propulsion Lab. (JPL), "Aviris free data," California Inst. Technol., Pasadena, CA, 2006. [Online]. Available: http://aviris.jpl.nasa.gov/html/aviris.freedata.html